Flow of viscoelastic fluids around a confined cylinder: comparison of standard and log-conformation stress formulations

A.M. Afonso[1], M.A. Alves[1], F.T. Pinho[2,3] and P.J. Oliveira[4]

[1]Departamento de Engenharia Química, Centro de Estudos de Fenómenos de Transporte, Faculdade de Engenharia da Universidade do Porto, Rua Dr. Roberto Frias, 4200-465 Porto, Portugal
email: aafonso@fe.up.pt ,mmalves@fe.up.pt, http://www.fe.up.pt
[2] Universidade do Minho, Largo do Paço, 4704-553 Braga, email: fpinho@dem.uminho.pt, http://www.uminho.pt
[3] Centro de Estudos de Fenómenos de Transporte, Faculdade de Engenharia da Universidade do Porto, Rua Dr. Roberto Frias, 4200-465 Porto, Portugal, email: fpinho@fe.up.pt, http://www.fe.up.pt
[4] Departamento de Engenharia Electromecânica, Universidade da Beira Interior, 6201-001 Covilhã, Portugal
email: pjpo@ubi.pt, http://www.ubi.pt

Abstract

A finite-volume method is applied to the numerical simulation of flows of viscoelastic fluids in the benchmark confined-cylinder problem under creeping flow conditions. The fluids are modeled using the Oldroyd-B constitutive equation, the calculation of the polymer stress contribution is carried out using the log-conformation methodology [1] and the results are compared with data using the standard method for calculating the polymer stress, as well as data from the literature. The log-conformation methodology allowed converged solutions at higher Deborah numbers flows than the standard method and was seen to be more stable.

Keywords: *Finite-volume; Log-conformation tensor; Viscoelastic; Cylinder flow.*

1 Introduction

A Finite Volume method (FVM) is applied to the numerical simulation of laminar viscoelastic flow around a confined cylinder. The Oldroyd-B fluid [2] was selected for this study, in order to allow direct comparison with previous works by Alves et al [3], and also to analyze the applicability of the matrix logarithm transformation [1] for Maxwell type models in a flow without geometric singularities.

The flow around a confined cylinder is a usual benchmark test-case in computational rheology. It is representative of fundamental flow dynamics of viscoelastic fluids around solid bodies and it can be encountered in many engineering processes. This flow has been studied experimentally by McKinley et al [4], Baaijens et al [5] and Shiang at al [6,7]. Owens and Phillips [8] documented and summarized the main numerical results, focusing primarily on the Oldroyd-B model. Although the flow around a confined cylinder is classified as a smooth flow, since it is free of geometric singularities, its numerical calculation presents some difficulties associated with the development of thin stress layers on the cylinder sidewall and along the centreline in the cylinder rear wake, imposing a limiting value to the Deborah number for which steady solutions can be obtained. In fact, the simulations for the cylinder flow with the Upper Convected Maxwell (UCM) or Oldroyd-B fluids are somehow limited by the so called High-Weissenberg Number Problem (HWNP; like the Deborah number, the Weissenberg number measures the flow elasticity). A breakdown in the calculations is found at a limiting Deborah number below 1 for the UCM fluid whereas for the Oldroyd-B fluid the breakdown occurs at higher Deborah numbers depending on the solvent viscosity ratio.

In order to get further insights into the HWNP, this work implements the methodology recently proposed by Fattal and Kupferman [1], the so called matrix-logarithm or log-conformation formulation (denomination used heretoforth) of the viscoelastic constitutive equations. This is based on a reformulation of the constitutive law in terms of the matrix logarithm of the conformation tensor. According to Fattal and Kupferman [1], this new formulation introduces a better polynomial interpolation of the logarithm of the variables that exhibit an exponential growth near stagnation points and also preserves the positive definiteness of the conformation tensor [1,9-15]. A similar logarithm transformation was used previously for scalar quantities in mass transfer problems by Miranda and Campos [16], who applied a simple logarithmic variable transformation to the solute transport to solve laminar flow and solute transport equations in a parallel plate device with permeable walls, improving their finite difference method and allowing the use of a larger grid spacing without loss of accuracy.

Fattal and Kupferman [1] reported a breakthrough in the HWNP in their numerical simulations with the Finitely-Extensible Nonlinear Elastic model using the Chilcott–Rallison approximation (FENE-CR) in a two-dimensional

lid-driven cavity flow. Later, Fattal and Kupferman [9] applied the log-conformation scheme to the flow of an Oldroyd-B fluid in the same geometry, using a multigrid solver and reported the possibility to perform stable simulations at very large values of the Weissenberg number. They included a stability criterion and stated that this condition may be very restrictive when convection is weak, as in creeping flows, and in the presence of large deformation rates, as in the flow around sharp corners. Recently, Pan and Hao [10] performed numerical simulations of the lid-driven cavity creeping flow for an Oldroyd-B fluid, using the finite element method (FEM). They also relied on the log-conformation technique, and found that this methodology is stable at high Weissenberg numbers, obtaining stable solutions up to *De*= 3.

Hulsen et al [11] were the first to implement the log-conformation methodology within the FEM framework and applied it to the benchmark flow of Oldroyd-B and Giesekus fluids past a confined cylinder. They reported an almost unbounded convergence limit for the Giesekus model, whereas for the Oldroyd-B fluid the solution became unsteady at high Deborah numbers, while exhibiting symptoms of strong mesh dependency particularly in the stress fields near the cylinder. Kwon [12] investigated numerically the planar 4:1 contraction flow with the Leonov constitutive equation and found stabler computations when using the log-conformation method than with the conventional approach. Kwon [12] also concluded that this new method may only work for constitutive equations that are proven globally stable and that the stability constraint has to be taken into serious consideration. In a sequel, Yoon and Kwon [13] obtained solutions for Deborah numbers in excess of 100 using finer meshes. These authors also presented solutions for the 4:1:4 contraction/expansion flow and obtained converged solutions for Deborah numbers above 10. However, in both geometries the convergence limits decreased with mesh refinement. More recently, Kwon [14] extended the log conformation formulation to the calculations of flows of Newtonian, non-Newtonian (Carreau model) and viscoelastic fluids in a channel obstructed by an asymmetric array of cylindrical obstacles. To express the viscoelastic nature of the liquid, a Leonov model was employed, obtaining stable solutions with an apparent unbounded convergence limit when the retardation parameter that specifies the solvent viscosity contribution was 0.5. In contrast, in the absence of a solvent contribution to the Leonov model, the limiting Deborah number becomes finite, between 4.5 and 20.

Coronado et al [15] used an alternative implementation of the log-conformation formulation in their simulations of the planar Couette flow and flow past a cylinder in a channel of several viscoelastic fluids. These were modeled by a generalized constitutive equation formulated in terms of the conformation tensor. Their results demonstrated that this alternative method works well for the generalized constitutive model improving the numerical stability at high *De*, especially in the flow past a confined cylinder, where the maximum *De* limit was extended to 1.0 as compared to 0.7 obtained with the standard DEVSS-TG/SUPG method. The results are also in good agreement with those presented by Hulsen et al [11].

The remainder of this paper is organised as follows: after presenting the governing equations the log-conformation modified constitutive equation is described. Then, we introduce the parameter used in this work to assess the loss of evolution phenomenon. Prior to the presentation of results the numerical method is briefly described and the geometry and computational meshes used for this flow problem are presented.

2 Governing equations

To simulate the steady incompressible flow of viscoelastic fluids, the following set of governing equations needs to be solved: conservation of mass,

$$\nabla \cdot \mathbf{u} = 0\,, \tag{1}$$

conservation of momentum,

$$\rho \frac{D\mathbf{u}}{Dt} = -\nabla p + \beta \eta_o \nabla \cdot \left(\nabla \mathbf{u} + \nabla \mathbf{u}^T\right) + \frac{\eta_o}{\lambda}(1-\beta)\nabla \cdot \mathbf{A}\,, \tag{2}$$

and a constitutive equation describing the evolution of the conformation tensor, **A**,

$$\mathbf{A} + \lambda \overset{\nabla}{\mathbf{A}} = \mathbf{I} \tag{3-a}$$

where $\overset{\nabla}{\mathbf{A}}$ represents the Oldroyd's upper-convected derivative of **A** given by equation 3-b, **I** is the unit tensor, **u** is the velocity vector, p is the pressure and λ is the relaxation time of the polymer.

$$\overset{\nabla}{\mathbf{A}} = \frac{D\mathbf{A}}{Dt} - \left(\mathbf{A}\cdot(\nabla \mathbf{u})^T + (\nabla \mathbf{u})\cdot \mathbf{A}\right) \tag{3-b}$$

The solvent viscosity ratio, β, is defined in equation (4) as the ratio between the Newtonian solvent viscosity, η_s, and the total zero shear rate viscosity, η_o,

$$\beta \equiv \frac{\eta_s}{\eta_o} = \frac{\eta_s}{\eta_s + \eta_P} \tag{4}$$

where η_p, is the contribution of the polymer to the zero-shear-rate viscosity.

For the Oldroyd-B model $0<\beta<1$ while for $\beta=0$ we recover the Newtonian constitutive equation. The constitutive law written in terms of the conformation tensor **A**, can be explicitly formulated as a function of the polymer contribution to the extra-stress tensor, $\boldsymbol{\tau}$, with the following relation valid for both models,

$$\boldsymbol{\tau} = \frac{\eta_p}{\lambda}(\mathbf{A}-\mathbf{I}) \tag{5}$$

and thus, the system of the governing equations can be written explicitly in terms of the extra stress tensor. Such formulation was followed in previous works [3,17-18], where the numerical methodology was extensively validated. Such approach, known as the standard method, is not used here except in some comparisons to assess the performance of the new log-conformation method.

2.1 The log-conformation representation

As mentioned above, Fattal and Kupferman [1] suggested a simple tensor-logarithmic transformation of the conformation tensor for differential viscoelastic constitutive equations, which can be applied to a wide variety of constitutive laws. The core feature of the transformation is the decomposition of the velocity gradient, $\nabla\mathbf{u}$, into a traceless extensional component, **E**, and a pure rotational component, **R**. With this decomposition, the constitutive law in equation (3), can be re-written as [1]

$$\frac{\partial \mathbf{A}}{\partial t} + (\mathbf{u}.\nabla)\mathbf{A} - (\mathbf{RA}-\mathbf{AR}) - 2\mathbf{EA} = \frac{1}{\lambda}(\mathbf{I}-\mathbf{A}), \tag{6}$$

In the log-conformation representation, equation (6) is replaced by an equivalent equation for the logarithm of the conformation tensor, $\boldsymbol{\Theta} = \log \mathbf{A}$, benefiting from the fact that **A** is a symmetric positive definite (SPD) matrix, and thus can always be diagonalized into the form [1]:

$$\mathbf{A} = \boldsymbol{\Omega}\mathbf{D}\boldsymbol{\Omega}^T = \boldsymbol{\Omega}^T\mathbf{D}\boldsymbol{\Omega}, \tag{7}$$

where $\boldsymbol{\Omega}$ is an orthogonal matrix made with the eigenvectors of matrix **A** and **D** is a diagonal matrix made with the corresponding three distinct eigenvalues of matrix **A**. The change from equation (6) to an equation for $\boldsymbol{\Theta} = \log \mathbf{A}$ is described in [1], and leads to

$$\frac{\partial \boldsymbol{\Theta}}{\partial t} + (\mathbf{u}.\nabla)\boldsymbol{\Theta} - (\mathbf{R}\boldsymbol{\Theta}-\boldsymbol{\Theta}\mathbf{R}) - 2\mathbf{E} = \frac{e^{-\boldsymbol{\Theta}}}{\lambda}(\mathbf{I}-e^{\boldsymbol{\Theta}}) = \frac{1}{\lambda}(e^{-\boldsymbol{\Theta}}-\mathbf{I}), \tag{8}$$

3 Numerical methods

In the past, our group adapted a Newtonian FVM to calculate viscoelastic flows where the polymer contribution to the extra-stress tensor was described by one of various differential rheological constitutive equations [3,17,18,21]. This fully-implicit FVM is based on a time-marching pressure-correction algorithm, formulated with the collocated variable arrangement, which is explained in detail in Oliveira et al [17] and Alves et al [18]. Here, the methodology is extended to the log-conformation procedure and the corresponding modifications are explained below.

The governing equations are first transformed to a non-orthogonal system, but keeping the Cartesian velocity and conformation/log-conformation components. The log-conformation tensor evolution equation (8) can thus be written into a general non-orthogonal coordinate system ($\zeta_1, \zeta_2, \zeta_3$) as,

$$\frac{\partial J\Theta_{ij}}{\partial t} + \frac{\partial}{\partial \zeta_k}\left(u_k \beta_{lk} \Theta_{ij}\right) = J\left(R_{ik}\Theta_{kj} - \Theta_{ik}R_{kj}\right) + 2JE_{ij} + \frac{J}{\lambda}\left(e^{-\Theta_{ij}} - \delta_{ij}\right). \tag{9}$$

After integration over the control volumes forming the computational mesh, and in time over a time step (δt), the coefficients β_{lk} are replaced by area components (index *k*) of the surface whose normal vector points towards direction *l*, the Jacobian *J* is replaced by the cell volume *V*, and the derivatives $\partial/\partial\zeta_l$ become differences between values along direction *l*. More details can be found in Oliveira et al [17].

Then, after the discretization the various terms are assembled, obtaining

$$a_P^{\Theta}\Theta_{ij,P} - \sum_F a_F^{\Theta}\Theta_{ij,F} = S_{\Theta_{ij}} + \frac{\lambda_P V_P}{\delta t}\Theta_{ij,P}^0, \tag{10}$$

where $\Theta_{ij,P}^0$ refers to the *ij* component of the log-conformation tensor at the previous time level, a_P^{Θ} represents the central coefficient, a_F^{Θ} represents the coefficients of the neighbouring cells (with F spanning the near-neighbouring cells of cell P) and $S_{\Theta_{ij}}$ is the total source term. The discretised momentum equations are solved sequentially after assembling all coefficients and source terms, to obtain the three Cartesian velocity components *u*, *v* and *w*. As generally the velocity components do not satisfy the continuity equation a pressure-correction

field, obtained from a Poisson pressure equation, is solved with a symmetric conjugate gradient method preconditioned with an incomplete LU decomposition.

The advective term in equation (8) was discretized with the high resolution scheme CUBISTA (Convergent and Universally Bounded Interpolation Scheme for the Treatment of Advection) of Alves et al [18], formally of third-order accuracy and especially designed for differential constitutive relations.

Table 1. Main characteristics of the Cylinder computational meshes.

	NC	*DOF*	*NR*	*NS*	$(\Delta r/R)_{min}$	$(\Delta s/R)_{min}$
$M30_{WR}$	22560	225600	30	260	0.008	0.0012
$M60_{WR}$	45120	451200	60	520	0.004	0.0006

NC- total number of cells; *DOF*- nº of degrees of freedom; *NR* – nº of cells placed radially; *NS* - nº of cells around the cylinder surface.

3.1 Computational meshes

The geometry of the viscoelastic fluid flow past a confined cylinder in a channel is shown in **Figure 1**. The ratio of channel half-height h to cylinder radius R is set equal to 2, which corresponds to the benchmark 50% blockage case. The computational domain is 200R long, with 99R upstream and 99R downstream of the forward and rear stagnation points of the cylinder, respectively. The downstream length is sufficient for the flow to become fully-developed and to avoid any effect of the outflow Newmann boundary condition upon the flow in the vicinity of the cylinder. Vanishing axial gradients are applied to all variables, including the pressure gradient, at the outlet plane. No-slip conditions are imposed at both the cylinder surface ($r=R$: $u=0$, $v=0$) and the channel wall ($y=\pm h$: $u=0$, $v=0$). The main characteristics of the meshes $M30_{WR}$ and $M60_{WR}$ used in this work are given in **Table 1**, including the total number of cells, (*NC*), the number of control volumes around the surface of the cylinder (*NS*), the number of cells placed radially from the cylinder to the channel wall (*NR*), and the minimum cell spacing normalized with the cylinder radius along the radial (Δr) and the azimuthal ($\Delta s=r\Delta\theta$) directions. The complete flow domain was mapped, in order to capture possible unsteady phenomena. The subscript WR (for wake-refined) is added to the mesh designation to denote a highly refined mesh along the wake. For $M30_{WR}$ the minimum normalized cell spacing along the azimuthal direction is of 0.0012 compared with 0.0314 for the equivalent mesh M30. Mesh $M60_{WR}$ has twice the number of cells along both directions as mesh $M30_{WR}$ with 45120 cells. The number of cells along the cylinder sidewall with that mesh is 560 and the minimum normalized cell spacing along the radial and azimuthal directions is 0.004 and 0.0006, respectively.

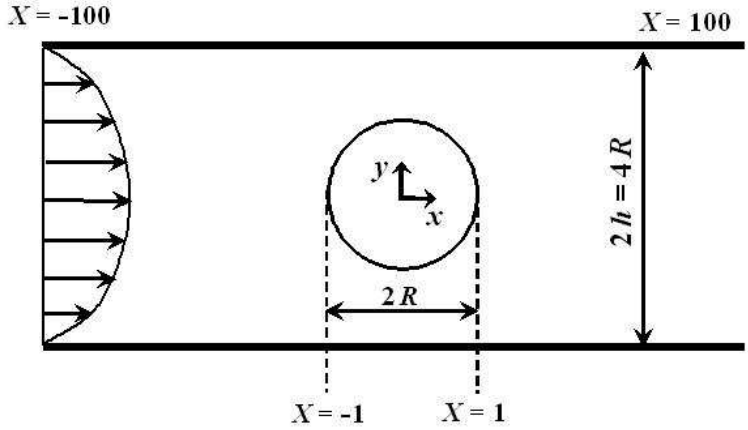

Figure 1. Schematic representation of the flow past a cylinder geometry ($X=x/R$).

4 Results

In order to analyze the performance of the log-conformation formalism in comparison with the standard formulation of the extra stress tensor, some flows were calculated with both formulations (for conciseness henceforth we denoted by ***StrT*** and ***LogT*** the results obtained with the standard and log-conformation, respectively). In all cases the L_2 norm of the residuals of the equations was required to be less than a tolerance of 10^{-6}, in order to stop the time stepping procedure.

All calculations were carried out at a vanishing Reynolds number, $Re=\rho RU/\eta_0=0$ (creeping flow) and we studied the effect of the Deborah number, here defined as

$$De = \frac{U\lambda}{R} \tag{11}$$

where λ is the relaxation time of the fluid and U and R represent the average velocity and the cylinder radius, respectively.

Results of computations are presented in two ways: as a scalar integral quantity representative of the whole flow; and as detailed profiles of velocity and stress components in the vicinity of the cylinder. The integral quantity is the dimensionless drag coefficient, C_D, calculated as:

$$C_D = \frac{1}{\eta_0 U}\int_S (\boldsymbol{\tau}_{tot} - p\mathbf{I})\cdot\mathbf{n}\cdot\mathbf{i}\,\mathrm{d}S \tag{12}$$

where **I** is the unit tensor, **n** is the unit vector normal to the cylinder surface and **i** is the unitary vector in the streamwise direction. Stress profiles are shown along the cylinder wall and on downstream rear wake, in order to ascertain the quality of the predictions. In this section we use the Oldroyd-B model with β=0.59. Normalization of the data is done as follows: coordinates were normalized by the cylinder radius, R, the velocity components using the characteristic velocity, U, and the total extra-stress tensor τ and the pressure p with $\eta_0 U/R$.

The positive definiteness of the conformation tensor is known to be crucial for well posedness of the evolution equation, although some degree of loss of evolution may be found in constitutive equations that have been proven to be stable under short and high frequency wave disturbances (Hadamard stability [19-20]).

One good criterion for judging the performance of the numerical discretization is to determine if the elastic tensor,

$$\mathbf{T} = \boldsymbol{\tau} + \frac{\eta_P}{\lambda}\mathbf{I} = \frac{\eta_P}{\lambda}\mathbf{A}, \tag{13}$$

is positive definite [19]. The matrix is said to be positive definite when all its eigenvalues are positive, and this can also be assessed by the system condition number, S, used to indicate temporal loss of evolution [20] (for 2D flow),

$$S = 2\frac{\lambda_1\lambda_2}{\lambda_1^2+\lambda_2^2} = 2\frac{\det\mathbf{T}}{\mathrm{tr}(\mathbf{T}^2)} = 2\frac{\lambda}{\eta_p}\frac{\det\mathbf{A}}{\mathrm{tr}(\mathbf{A}^2)}, \tag{14}$$

where λ_1 and λ_2 are the non trivial eigenvalues of tensor **T**. Note that if one of the invariants of **A** ($\det\mathbf{A}$ and $\mathrm{tr}(\mathbf{A}^2)$) is negative, the positive definiteness of tensor **A** is violated.

The simulations with the ***StrT*** formulation diverged at De=0.9 with mesh $M60_{WR}$. The loss of positive definiteness is most probably the main cause of this divergence, as observed in **Figure 2**, where the minimum value of the system condition number and the absolute value of the determinant of the conformation tensor are presented. After approximately two relaxation times, the simulation with the ***StrT*** formulation begins to present negative values of S_{min}. As $\mathrm{tr}(\mathbf{A}^2)$ is a positive scalar, S_{min} can only become negative due to negative values of the $\det(\mathbf{A})_{\min}$ (c.f. equation (10)), i.e., at least one of the eigenvalues of **A** becomes negative. For the ***LogT*** formulation the values of S_{min} and $\det(\mathbf{A})_{\min}$ are always positive, showing no signs of loss of evolution.

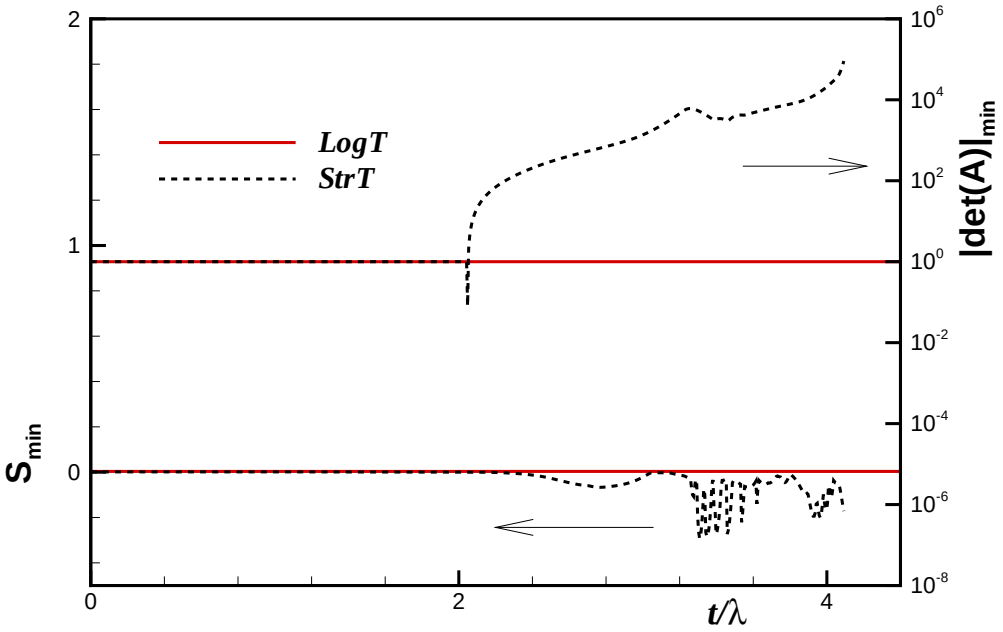

Figure 2. Evolution of the minimum stability factor (S_{min}) and $\left|\det(\mathbf{A})_{\min}\right|$ for an Oldroyd-B fluid (β=0.59) in the inertialess flow past a cylinder for both ***StrT*** and ***LogT*** formulations at De=0.9 with mesh $M60_{WR}$.

The literature data for the dimensionless drag coefficient show some discrepancies, especially for Deborah numbers above 0.7. Alves et al [3] used the standard method employing highly refined non-orthogonal meshes which allowed a good comparison of the predicted drag force with values from other simulations in the literature [11,15,21-22]. In particular, their predictions of C_D were nearly identical to those of the FEM simulations of Fan et al [21]. The predictions of drag force of Kim et al [22] also agreed well with the previous results up to De=0.9.

The predictions of C_D in this work are presented in **Figure 3**. Up to De= 0.9 the results agree well with the data of Alves et al [3], Fan et al [21], Kim et al [22] and Hulsen et al [11]. For higher Deborah numbers, no steady state could be attained, with the C_D values oscillating in time with the amplitude marked as error bars in **Figure 3**. Here, instead of using the value of C_D right after the onset of the transient behaviour, as used in the work of Hulsen et al [11], the plotted quantity is the time-averaged C_D value. Although the mean values for both meshes are slightly higher than the predictions of Hulsen et al [11], the lower bound of the oscillations are in agreement with the latter's predictions.

In terms of stress convergence with mesh refinement, it is well known that for De>0.7 significant discrepancies are found among the results from the literature [3,11,15,21-22], especially in the maximum peak values of the normal stress component at the rear wake. Even the results of the extra stresses obtained with highly refined meshes at the rear stagnation region using high order method [3,21,22] are not conclusive in this respect.

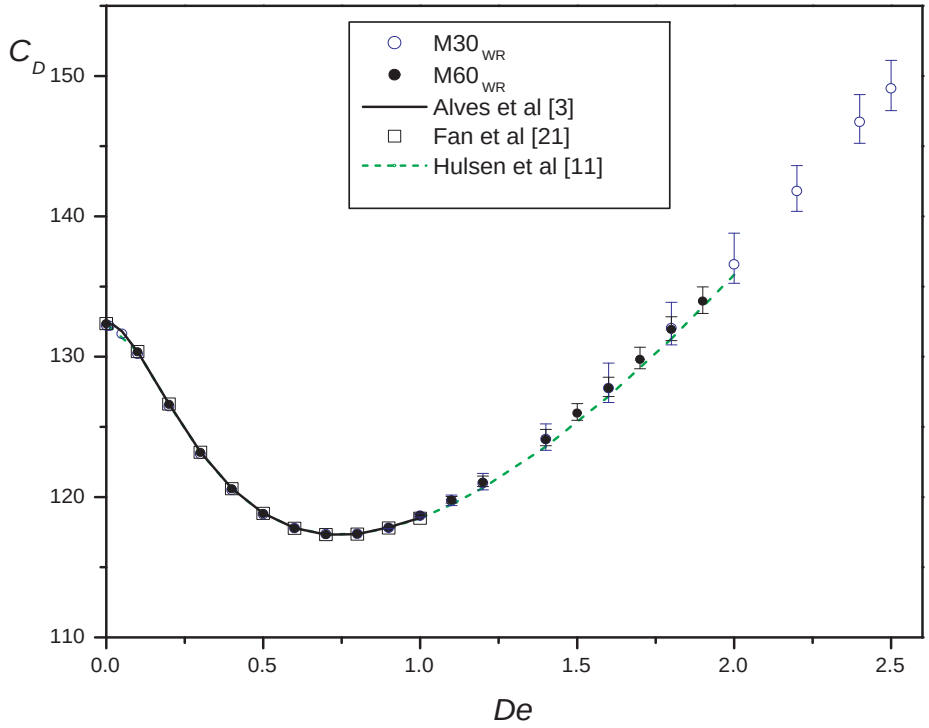

Figure 3. Drag force coefficient for an Oldroyd-B fluid (β=0.59) in the inertialess flow past a cylinder. ***LogT*** formulation with meshes $M30_{WR}$ and $M60_{WR}$ and with data from literature.

Figure 4 shows normal stress profiles along the surface and the rear wake as obtained with different meshes at De=0.6; the results are practically mesh independent, but in the rear wake they are slightly above those of Alves et al [3] using the ***StrT*** formulation (in this section, we use the results of Alves et al [3] in their refined mesh M120 to represent the ***StrT*** formulation). This difference is due to the refinement of the mesh in the wake allowing the stresses to be better resolved in meshes $M30_{WR}$ and $M60_{WR}$ than in mesh M120, thus showing the advantage of wake refined meshes. Further increase in Deborah number to De=0.9 enhances the discrepancies in the rear wake zone, as shown in **Figure 5**. Although on the cylinder surface the normal stress peaks obtained with the ***LogT*** and mesh $M60_{WR}$ are in close agreement with the results of Alves et al [3] for mesh M120 and ***StrT***, in the rear wake the differences are large. There is also a well marked discrepancy in relation to the data of Fan et al [21] and Coronado et al [15].

In this work, unsteady solutions were obtained for Deborah numbers from 1.0 up to 3.0 and 1.9, for meshes $M30_{WR}$ and $M60_{WR}$, respectively. This represents an increase of about 90% in the maximum attainable De as one goes from the ***StrT*** to the ***LogT*** formulation. Using the last approach, the stability requirements were always attained, and no signs of loss of evolution were found, with the minimum values of S and det(**A**) being always positive.

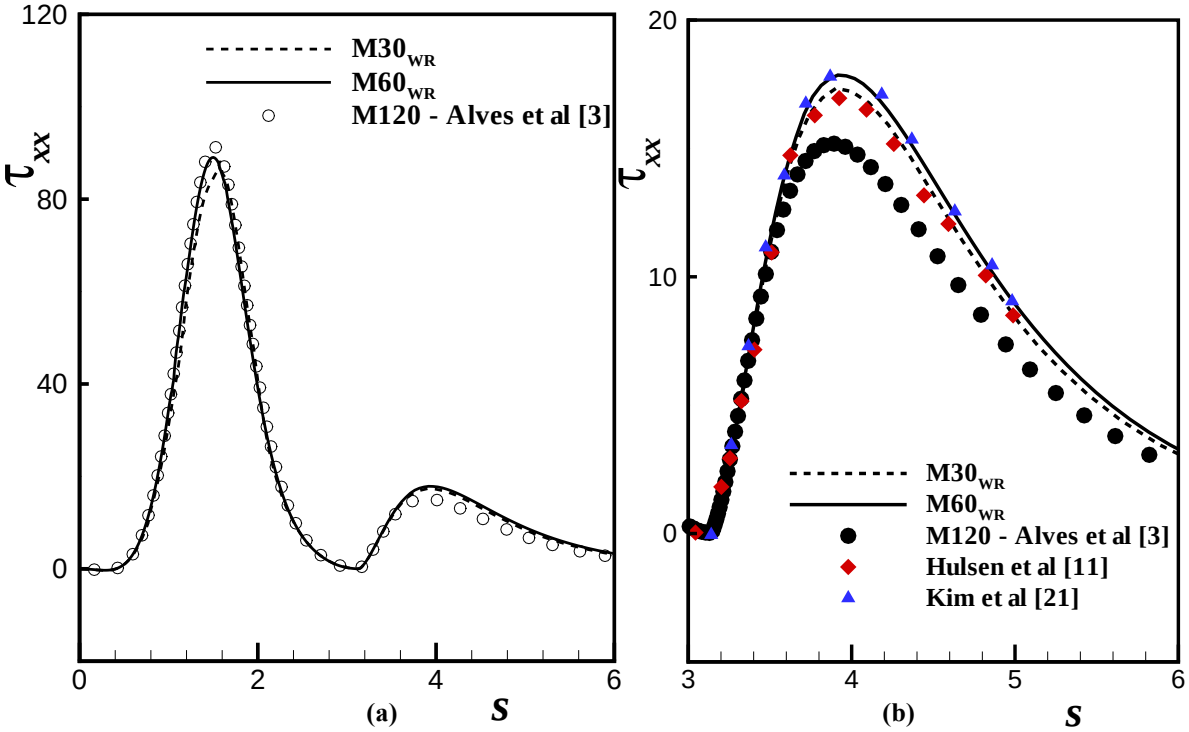

Figure 4. Effect of mesh refinement: (a) stress profiles along cylinder wall and downstream centreplane for an Oldroyd-B fluid at De=0.6. ***LogT*** formulation with meshes M30$_{WR}$ (dashed line) and M60$_{WR}$ (full line), and comparison with literature data. (b) Closer view in the rear wake of the cylinder.

To obtain further insights into the time-dependent flow, calculations were carried out using a second-order time discretization scheme [23] in order to increase the precision. **Figure 6** (a) shows the time evolution of C_D using different time steps for De=1.2 and mesh M30$_{WR}$. The solutions obtained with the smaller time steps, ($\Delta t/\lambda$=4x10^{-5}and $\Delta t/\lambda$=2x10^{-5}) collapse and are independent of $\Delta t/\lambda$, showing good time accuracy. The normal stress profiles at four different moments of time are plotted in **Figure 6** (b) and show a very sharp increase in τ_{xx} near the rear stagnation point at some moments of time, thus breaking the smoothness of the stress profile in this viscoelastic flow. This reveals the major importance of the minimum mesh size in the axial direction in the stagnation point region. Although stable results were obtained up to De=1.8 by Hulsen et al [11] they also presented symptoms of stress convergence problems for De>0.7, suggesting that a possible reason was that the length scale associated with the changes of the velocity gradient near the stagnation point was much smaller than the minimum mesh size in their most refined mesh. Hulsen et al [11] questioned the existence of a smooth solution near the cylinder and recently Renardy [24] suggested that at high Deborah number flows the smoothness of viscoelastic stresses could be expected to deteriorate.

5 Conclusions

A finite-volume method was adapted to the log-conformation formulation of Fattal and Kupferman [1] and applied to the simulation of 2D laminar viscoelastic flow around a confined cylinder using the Oldroyd-B model. In spite of the usual stress convergence problems in the confined cylinder geometry, the calculations with the log-conformation were more stable than those using the standard stress formulation and exceeded the usual critical Deborah number by a factor of 90% when using mesh M60$_{WR}$ and by a factor of 3 with mesh M30$_{WR}$. For higher Deborah numbers, sharp profiles are observed for τ_{xx} near the stagnation point, breaking the smoothness of the stress profile and revealing the major importance of refinement in the axial direction at the rear stagnation region of the cylinder.

6 Acknowledgements

The authors acknowledge funding from FEDER and Fundação para a Ciência e a Tecnologia (FCT) through projects POCI/EQU/59256/2004, POCI/EQU/56342/2004 and PTDC/EME-MFE/70186/2006. A. Afonso would also like to thank FCT for financial support through scholarship SFRH/BD28828/2006.

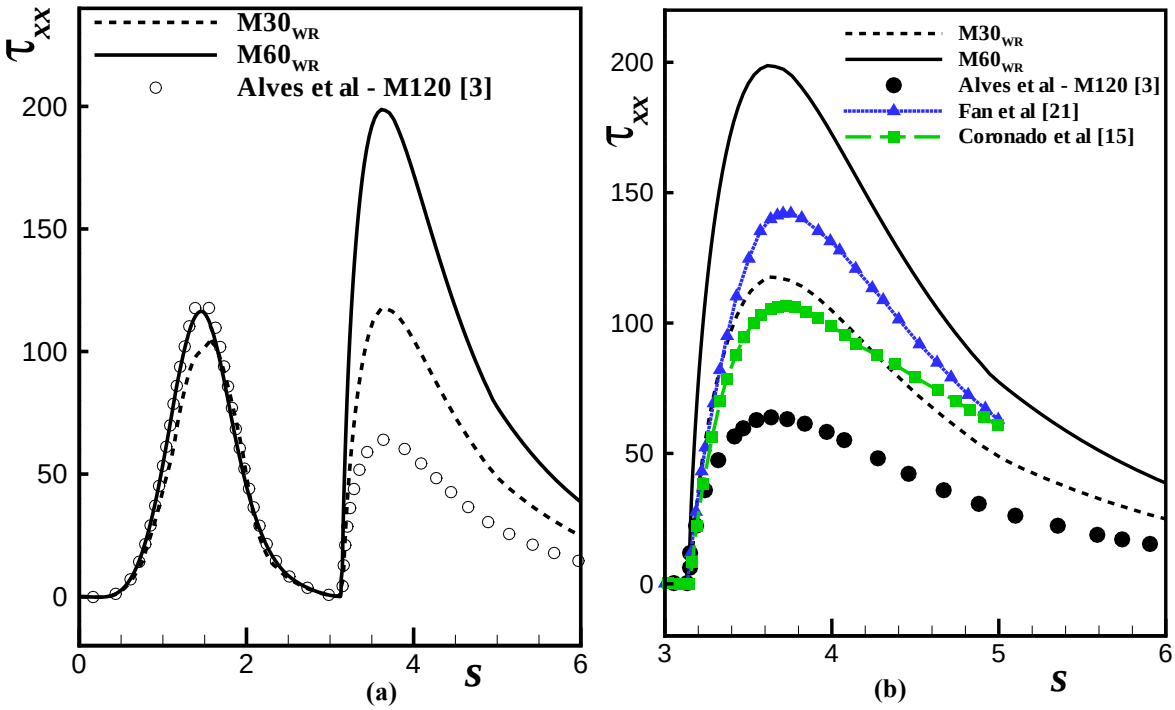

Figure 5. Effect of mesh refinement: (a) stress profiles along cylinder wall and downstream centreplane for an Oldroyd-B fluid at *De*=0.9. ***LogT*** formulation with meshes $M30_{WR}$ (dashed line) and $M60_{WR}$ (full line), and comparison with literature data. (b) Closer view in the rear wake of the cylinder.

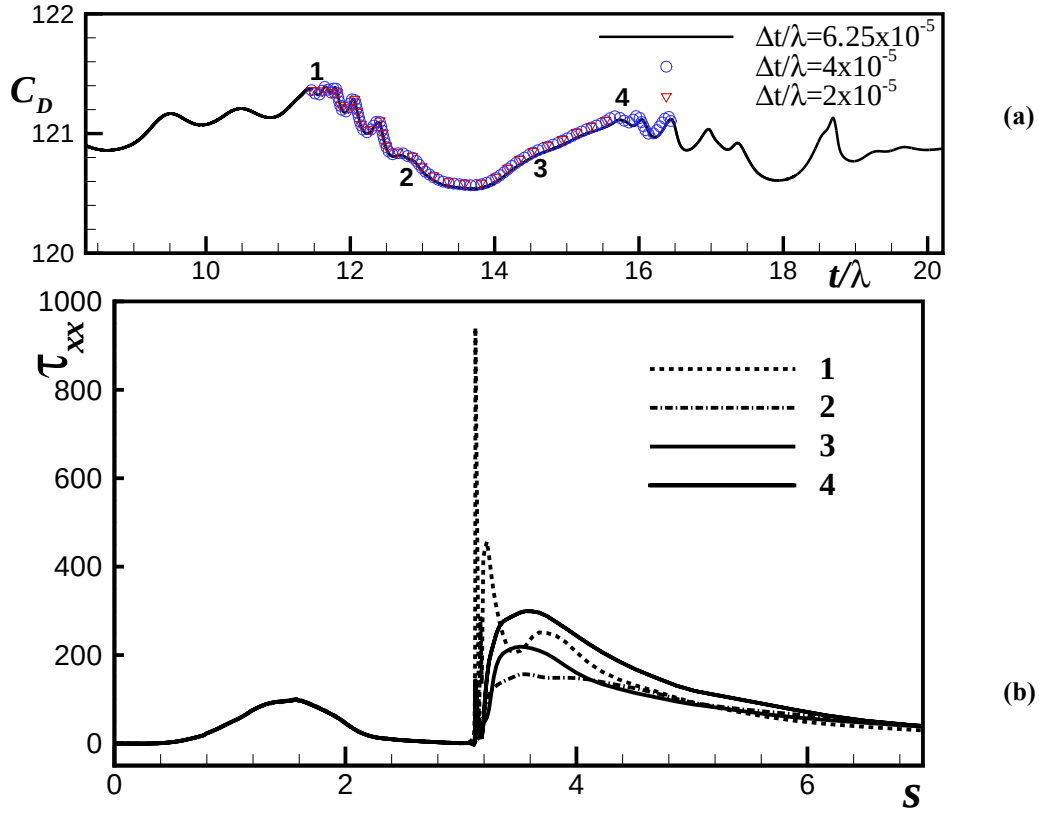

Figure 6. (a) Time evolution of C_D for several $\Delta t/\lambda$, (b) stress profiles along cylinder wall and downstream centreplane at the four instants of time marked in (a). Oldroyd-B fluid (β=0.59) at *De*=1.2 in Mesh $M30_{WR}$.

References

1. R. Fattal and R. Kupferman, Constitutive laws of the matrix-logarithm of the conformation tensor, J. Non-Newtonian Fluid Mech. 123 (2004), 281-285.
2. J.G. Oldroyd, On the formulation of rheological equations of state, Proc R Soc Lond, A200 (1950) 523–541.
3. M.A. Alves, F.T. Pinho and P.J. Oliveira, The flow of viscoelastic fluids past a cylinder: Finite-volume high-resolution methods. J Non-Newtonian Fluid Mech 97 (2001), 207-232.
4. G.H. McKinley, R.C. Armstrong and R.A. Brown, The wake instability in viscoelastic flow past confined circular cylinders, Philos Trans R Soc Lond A, 344 (1993), 265–304.
5. F.P.T. Baaijens, H.P.W. Baaijens, G.W.M. Peters, H.E.H. Meijer, An experimental and numerical investigation of a viscoelastic flow around a cylinder, J. Rheology 38 (1994) 351:376
6. A.H. Shiang, J.C. Lin, A. Öztekin and D. Rockwell, Viscoelastic flow around a confined circular cylinder: measurements using high image-density particle image velocimetry. J Non-Newtonian Fluid Mech 73 (1997), 29-49.
7. A. H. Shiang, A. Öztekin, J.C. Lin and D. Rockwell, Hydroelastic instabilities in viscoelastic flow past a cylinder confined in a channel, Experiments in Fluids, 28 (2000), 128-142.
8. R.G. Owens and T.N. Phillips, Computational Rheology, Imperial College Press, London, (2002).
9. R. Fattal and R. Kupferman, Time-dependent simulation of viscoelastic flows at high Weissenberg number using the log-conformation representation. J. Non-Newtonian Fluid Mech., 126 (2005) 23–37.
10. T.W. Pan and J. Hao, Numerical simulation of a lid-driven cavity viscoelastic flow at high Weissenberg numbers, C. R. Acad. Sci. Paris, Ser. I 344 (2007).
11. M. A. Hulsen, R. Fattal and R. Kupferman, Flow of viscoelastic fluids past a cylinder at high Weissenberg number: Stabilized simulations using matrix logarithms, J. Non-Newtonian Fluid Mech. 127 (2005), 27-39.
12. Y. Kwon, Finite element analysis of planar 4:1 contraction flow with the tensor-logarithmic formulation of differential constitutive equations, Korea-Australia Rheology J. 16 (2004), 183-191.
13. S. Yoon and Y. Kwon, Finite element analysis of viscoelastic flows in a domain with geometric singularities, Korea-Australia Rheology J., 17 (2005), 99-110.
14. Y. Kwon, Numerical analysis of viscoelastic flows in a channel obstructed by an asymmetric array of obstacles, Korea-Australia Rheology J., 18 (2006), 161-167.
15. O. M. Coronado, D. Arora, M. Behr and M. Pasquali, A simple method for simulating general viscoelastic fluid flows with an alternate log-conformation formulation, J Non-Newtonian Fluid Mech 147 (2007) 189-199.
16. J.M. Miranda, J.B.L.M. Campos, An improved numerical scheme to study mass transfer over a separation membrane, Journal of Membrane Science 188 (2001), 49–59.
17. P.J. Oliveira, F.T. Pinho and G.A. Pinto, Numerical simulation of non-linear elastic flows with a general collocated finite-volume method, J. Non-Newtonian Fluid Mech. 79 (1998), 1–43.
18. M.A. Alves, P.J. Oliveira and F.T. Pinho, A convergent and universally bounded interpolation scheme for the treatment of advection, Int J Num Methods in Fluids, 41 (2003) 47.
19. F. Dupret, J.M. Marchal, Loss of evolution in the flow of viscoelastic fluids. J Non-Newtonian Fluid Mech 20 (1986)143–171.
20. S.J. Lee, S.Yoon, Y. Kwon and S.J. Kim, Practical comparison of differential viscoelastic constitutive equations in finite element analysis of planar 4:1 contraction flow. Rheol. Acta 44 (2004) 188–197.
21. Y. Fan, R.I. Tanner and N. Phan-Thien, Galerkin/least-square finite-element methods for steady viscoelastic flows. J Non-Newtonian Fluid Mech 84 (1999), 233–256.
22. J.M. Kim, C. Kim, K.H. Ahn, S.J. Lee, An efficient iterative solver and high precision solutions of the Oldroyd-B fluid flow past a confined cylinder. J Non-Newtonian Fluid Mech 123 (2004), 161–173.
23. P.J. Oliveira, Method for time-dependent simulations of viscoelastic flows: vortex shedding behind cylinder, J. Non-Newtonian Fluid Mech. 101 (2001) 113–137.
24. M. Renardy, A comment on smoothness of viscoelastic stresses, J. Non-Newtonian Fluid Mech. 138 (2006) 204–205.